ISSN 0016-8521, Geotectonics, 2022, Vol. 56, No. 2, pp. 200–211. © Pleiades Publishing, Inc., 2022.
ISSN 0016-8521, Geotectonics, 2022. © Pleiades Publishing, Inc., 2022.

Structural Analysis of the Coal-Bearing Kleidi Basin: Insights in Kinematics of the Broader Ptolemais Sedimentary Basin (Western Macedonia, Greece)

C. D. Athanassas[a, *], D. Ntokos[a], and C. Roumpos[b]

[a] *Laboratory of Geology, Department of Geological Sciences, School of Mining and Metallurgical Engineering, National Technical University of Athens (NTUA), Zografos, 15780 Athens, Greece*

[b] *Public Power Corporation of Greece, Mining Engineering Department, 10432 Athens, Greece*

**e-mail: athanassas@central.ntua.gr*

Received June 12, 2021; revised November 21, 2021; accepted January 27, 2022

Abstract—This study processes borehole data from the coal-bearing Kleidi basin (Ptolemais sedimentary basin, Western Macedonia, Greece) to unravel the timeline of the neotectonic configuration of the basin and correlate it with the neotectonics of the broader region. Coal (lignite) deposits preserve faulted sequences, and for this reason they are ideal locations for studying deformation patterns. Lithostratigraphic data acquired by previous investigations revealed a continuous stratigraphic sequence which spans from the Upper Miocene to the Middle Quaternary. These Neogene deposits demonstrate their maximum thickness towards the SE of the basin. Boreholes also revealed that in the subsurface, the basin is actually divided into two separate grabens on either side of a ridge of the alpine basement. Stratigraphic interpolations using the inverse distance algorithm-generated thickness rasters which, through successive derivation, allowed the discovery of normal faults. Repetition of the algorithm using the new structural constraints returned patterns of deformation in the southern part of the Kleidi basin different from those revealed in the northern part. The configuration of the southern part of the Kleidi basin seems to reflect the Late Miocene–Pliocene extensional event. In contrast, configuration of the northern part of the basin is compatible with a later extensional phase in Pliocene–Quaternary. Both events are manifested in the tectonostratigraphy of the Ptolemais sedimentary basin and the broader area.

Keywords: rifting, geologic structure, neotectonics, sedimentary basin, kinematics, stratigraphy, normal faulting, extension

DOI: 10.1134/S0016852122020078

INTRODUCTION

Located in Western Macedonia (Greece) coal (lignite) deposits preserve faults at several scales. If the stratigraphy is adequately constrained from excavations or boreholes, coal mines are suitable sites for the study of the geometry and kinematics of dip-slip, high-angle faults based on marker horizon offsets [3, 21, 27, 32. 35]. In Greece, the hinterland of the Hellenic orogen was dissected by a myriad of normal faults at several scales during the Neogene–Quaternary period [4, 20]. The resulting continental depressions received a significant amount of organic remains from their surrounding biomes, favoring the formation of substantial coal deposits in lacustrine basins. On the Greek mainland, such major coal-bearing basins include the Megalopolis, Drama, Florina, and Ptolemais basins and exploitation of their deposits has shaped the energy landscape of Greece over the past decades [12, 22].

Specifically, in Northern Greece, the neotectonic depressions which have formed much of the Ptolemais sedimentary basin (Western Macedonia, Greece) initiated in the Late Miocene and resulted from a major NE–SW extensional phase [17, 25] (Fig. 1). Later, they were affected by a subsequent NW–SE extensional event during the Pleistocene. The latter segmented the broader basin into smaller grabens, which accommodated a great volume (up to 600 m thick) of lacustrine deposits [17, 25]. The NW corner of the broader Ptolemais basin is occupied by the Kleidi coal deposit. The open-cast coal mine, which has been developed for the exploitation of this deposit, is inactive because of the current specific mining, geotechnical, and economic conditions related to electricity generation from coal.

Kleidi basin has been surveyed as a potential coal mine in previous decades [7, 15]. Boreholes and detailed plans produced by mining surveyors, from the Institute of Geological and Mineral Exploration ((IGME), Athens, Greece) and Public Power Corporation of Greece ((PPC), Athens, Greece) [6, 7, 15].

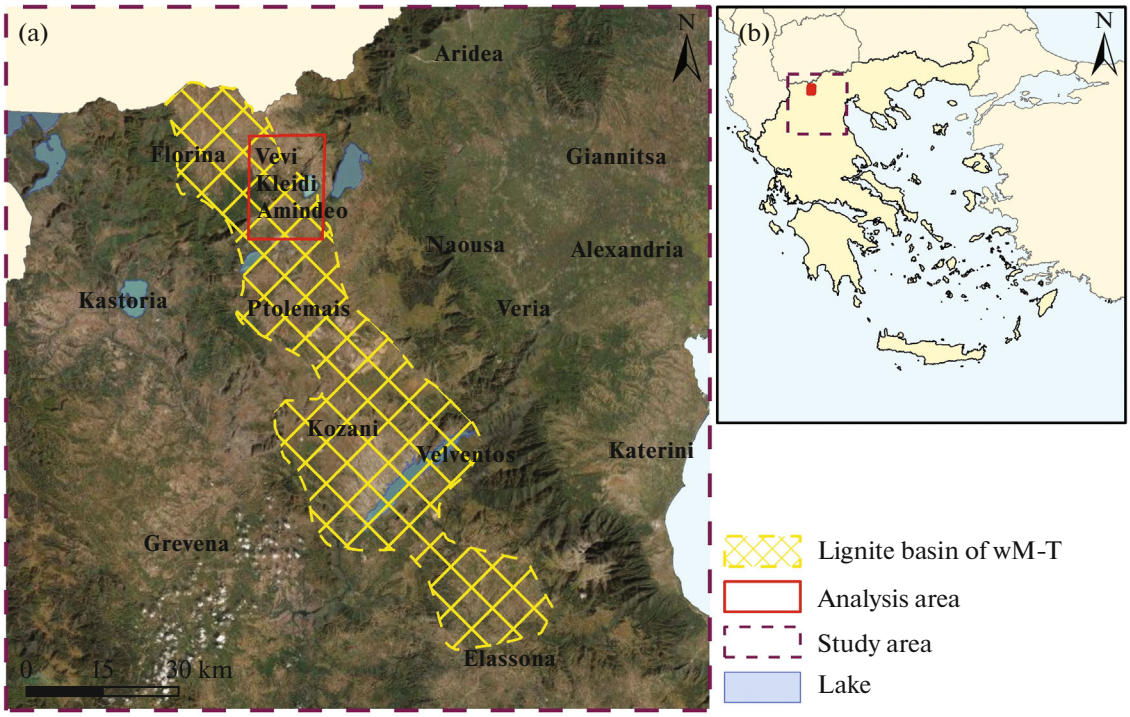

Fig. 1. Physiographic map of NW Greece and the broader Ptolemais sedimentary basin (after [13], plotted on the Qgis satellite basemap). Insets: position of the Kleidi mine in the broader Ptolemais sedimentary basin (a) showing the Ptolemais sedimentary basin (yellow checkered area); study area (orange color) and the map of Greece (b).

In 1997 and 2012, during two separate campaigns, data were obtained and they are here utilized for stratigraphic correlations to produce a structural model of the sedimentary basin and identify dip-slip faults crisscrossing the basin at depth below the featureless ground surface. Given the phase-out of coal mining operations as a result of the decarbonization, investigation of the stratigraphy and the geologic structure of the Kleidi deposit and the broader region may also become an essential part of reclamation works and post-mining activities. Nevertheless, exploration of the tectonic fabric of a sedimentary basin through stratigraphic modeling of borehole data is a rather challenging research issue [14, 23, 33]. In this study we take advantage of the core data retrieved by the previous campains to calculate a structural model of the Kleidi basin. Specifically, interpolation of chronostratigraphic markers across the basin will allow detecting structural discontinuities, that is faults, whose relative chronology and amount displacement will be contrasted against the well-documented history of neotectonic deformation of the broader area.

GEOLOGIC SETTING

Across the broader Ptolemais sedimentary basin, the post-alpine stratigraphy can be generalized into four lithostratigraphic units, conformably deposited one onto another [1, 28, 29] (Fig. 2). The same stratigraphy holds for the Kleidi basin except that the units vary as to their thickness. The generalized stratigraphy for the Kleidi basin is displayed in Fig. 3. A 94-m thick basal formation, consisting of alternating silts, sands, and conglomerates, unconformably lies over the basement bedrock (Pelagonian crystalline limestones, dolomites and, occasionally, metamorphic rocks such as marbles and gneiss) and marks the initiation of the Neogene sedimentation in the basin. The basal formation goes over the Lower Unit: a ~250-m thick sequence of alternating clastic deposits (clays, silts, sands, cobbles, and conglomerates) accommodating a ~97-m thick lignite deposit (Fig. 3). The unit dates from the Upper Miocene to the Lower Pliocene [30]. The sequence continues upsection with the 102-m thick Upper Unit: alternating layers of clays, marls and sands, chronologically spanning from the Early Pliocene to the Late Pliocene (Fig. 3). The Upper Unit accommodates a 53-m thick lignite deposit. Finally, the stratigraphic column is capped by thick (~119 m) Quaternary deposits, which are usually coarser than the underlying stratigraphic units and consist of conglomerates, cobbles and generally coarse clasts strewn into a finer (silty to clayey) matrix.

Regarding the tectonic fabric, the Kleidi basin is a part of the broader basin that stretches from Kozani and, through Ptolemais and Florina, terminates at the northern border of Greece (Fig. 1). The basin is bound by NW–SE trending normal faults (and their conjugate ones at right angles) initiated during the Late Miocene-Pliocene period and their orientation

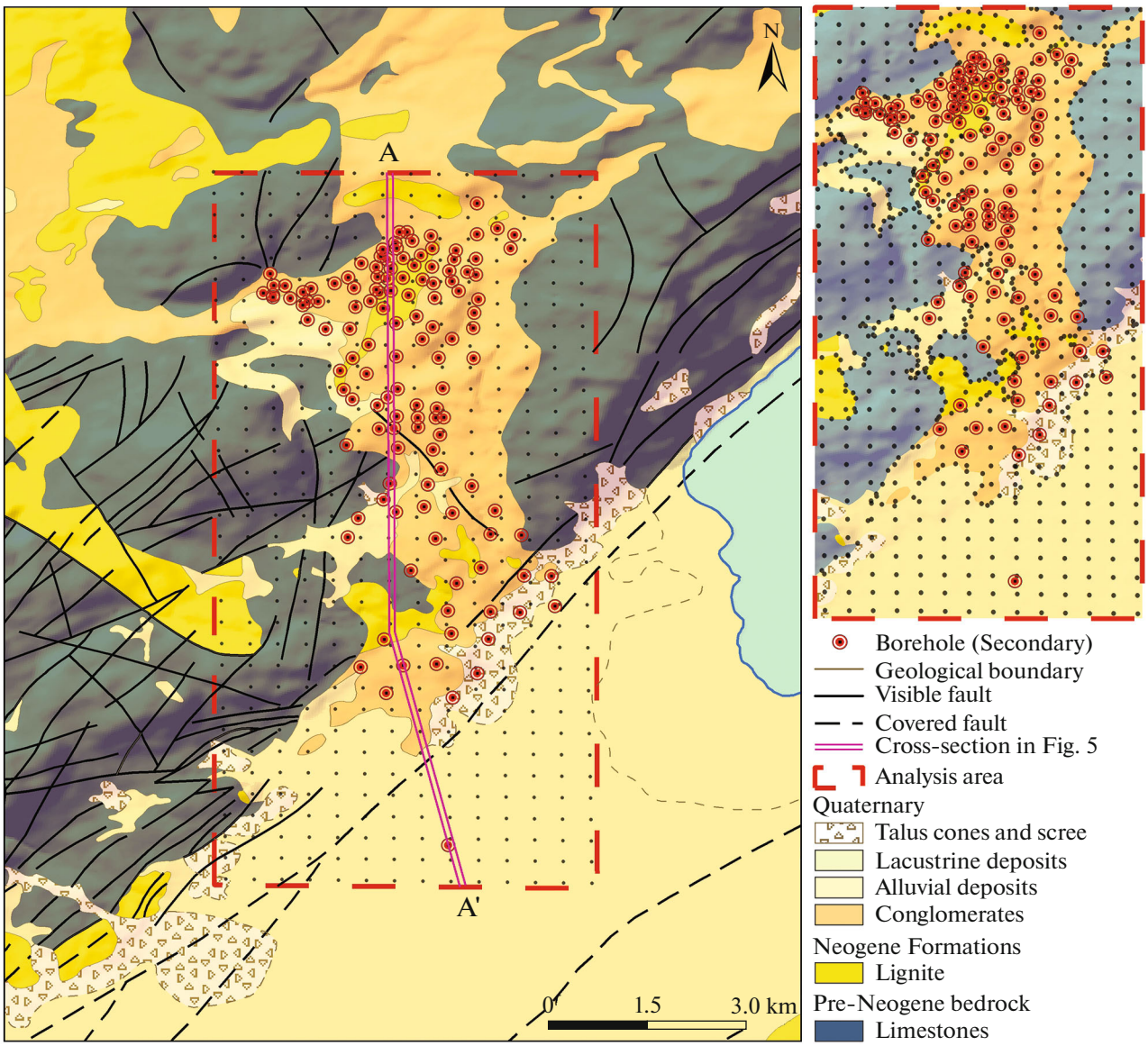

Fig. 2. Geological map of the Kleidi basin (study area) and the surrounding area in the NE part of the broader Ptolemais basin (after [7, 13], modified), showing the position of boreholes retrieved during the 1997 (IGME) and 2012 (PPCG) investigations (red concentric circles); north-south geological cross-section (double red line).

implies a NE–SW stretching direction. The subsequent generation of NE–SW trending faults was activated during the Late Pliocene–Middle Pleistocene, associated with the NW–SE extension event [11, 18, 25, 26]. Throws associated with normal faulting range from a few centimeters up to a few hundreds of meters.

METHODS AND DATA

Coring in the Kleidi area was undertaken by the Institute of Geology and Mineral Exploration (Athens, Greece) during 1991–1997 and the Engineering Department of the Public Power Corporation S.A. (PPC, Athens, Greece), during 2012 [6, 7, 13]. In total, 128 boreholes were drilled over the area of 33 km^2 at positions designated by a 400 × 400 m grid (Fig. 2). Coring was intended to meet the pre-Neogene bedrock (carbonates and metamorphics). However, it was carried out to depths down to ~350 m where the boreholes indeed encountered hard rocks but given the depth of coring, they more likely corresponded to intercalating boulders rather than the pre-Neogene bedrock.

Gridding

Gridding employed the Inverse-Distance (ID) method, executed in Rockworks [36]. We used one of the most popular deterministic algorithms used in the 3D modeling of geological structures, natural disasters as well as ore deposits [8, 15, 19, 34]. In the ID

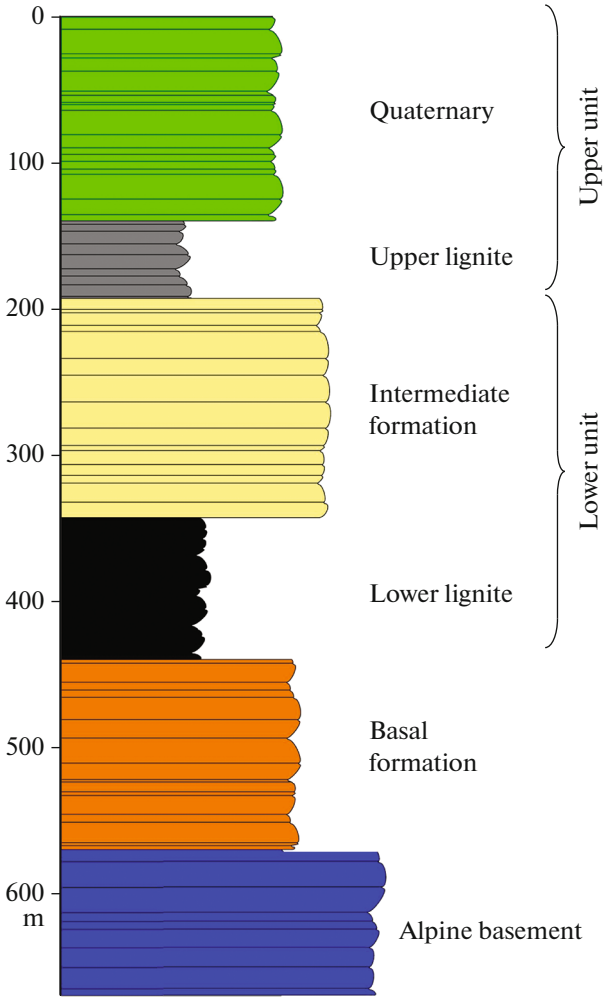

Fig. 3. Generalized stratigraphy of the Kleidi basin (after [13], modified).

method, each node of the grid receives the weighted average of all data points where the value of each data point is weighted according to the inverse of its distance from the grid node, raised to the *n*th power:

$$z = \frac{\sum \frac{z}{d^n}}{\sum \frac{1}{d^n}}, \quad (1)$$

Z corresponds to the value of the node, and z corresponds to the value of the data point. The greater than one the power raising the distance factor in the denominator the less influence the values of distant data points will exert on the value assigned to the grid node than neighboring points (thus resulting in smooth interpolated surfaces). All data points were used to compute the grid node value in order to prevent concentric closed contours from forming around control points.

Core logging revealed strongly alternating lithologies, showing the entire spectrum of clastic sedimentation and strong lateral heterogeneity. With the exception of the distinct lignite markers, the strongly variable lithology complicates stratigraphic correlations across the basin in a way that specific horizons in conventional cross-sections give the false impression of having moved reversely in an overall dip-slip fault setting, misguiding the tracing of faults across the basin, (i.e., introduction of false positives in geological mapping) [6]. Consequently, for the 3D reconstruction of the basin we preferred to group the alternating clastic lithologies per borehole into broader stratigraphic units, following the generalized stratigraphy shown in Fig. 3, while ensuring accurate placement of the distinct lignite marker horizons in the model. In order to delineate in the 3D model the perimeter of the cored deposits at the ground surface as they wedge out towards the bedrock, 930 virtual boreholes (0.2 m deep each) were fixed on the geological boundary shown in the geological map, encircling the actual boreholes.

Percentage of Stratigraphic Interval Change

Listric or rotational-fault-block modes of extensional tectonics during synrift sedimentation will produce a rollover anticline in the hanging wall [5, 35]. Contrary to the shear-thinning during nondeposition, the curved portion of the beds in synrift sequences forms a wedge in the hangingwall, which thickens towards the fault plane in either case. A relative chronology for the fault activity can be displayed through graphs that plot the percentage interval change versus the chronostratigraphy [2, 35]:

$$I = \frac{I_h - I_f}{I_f} \times 100, \quad (2)$$

where I_f is the thickness of a bed in the footwall of an extension fault and I_h is the thickness of the same bed in the hanging wall. If I is plotted against the stratigraphic age for all beds, then the maxima in the resulting curve will correspond to intervals of maximum fault activity in the synrift sequence. In this study, I was calculated across faults deduced from the interpolated stratigraphy to explore their activity during the Neogene.

KLEIDI BASIN 3D RECONSTRUCTION

3D reconstruction of the Kleidi basin stratigraphy, as calculated from the borehole interpolation, is presented (Fig. 4, fence diagram). Figure 5 provides another perspective of the interpolated stratigraphy in the form of a NW–SE geological cross-section. The sinuous basin floor slopes southwards, and the intrabasin Neogene deposits tend to thicken towards the SE. Coring also revealed a subsurface ridge of the basement, which divides the basin into two grabens: the northern graben and the southern graben, with the

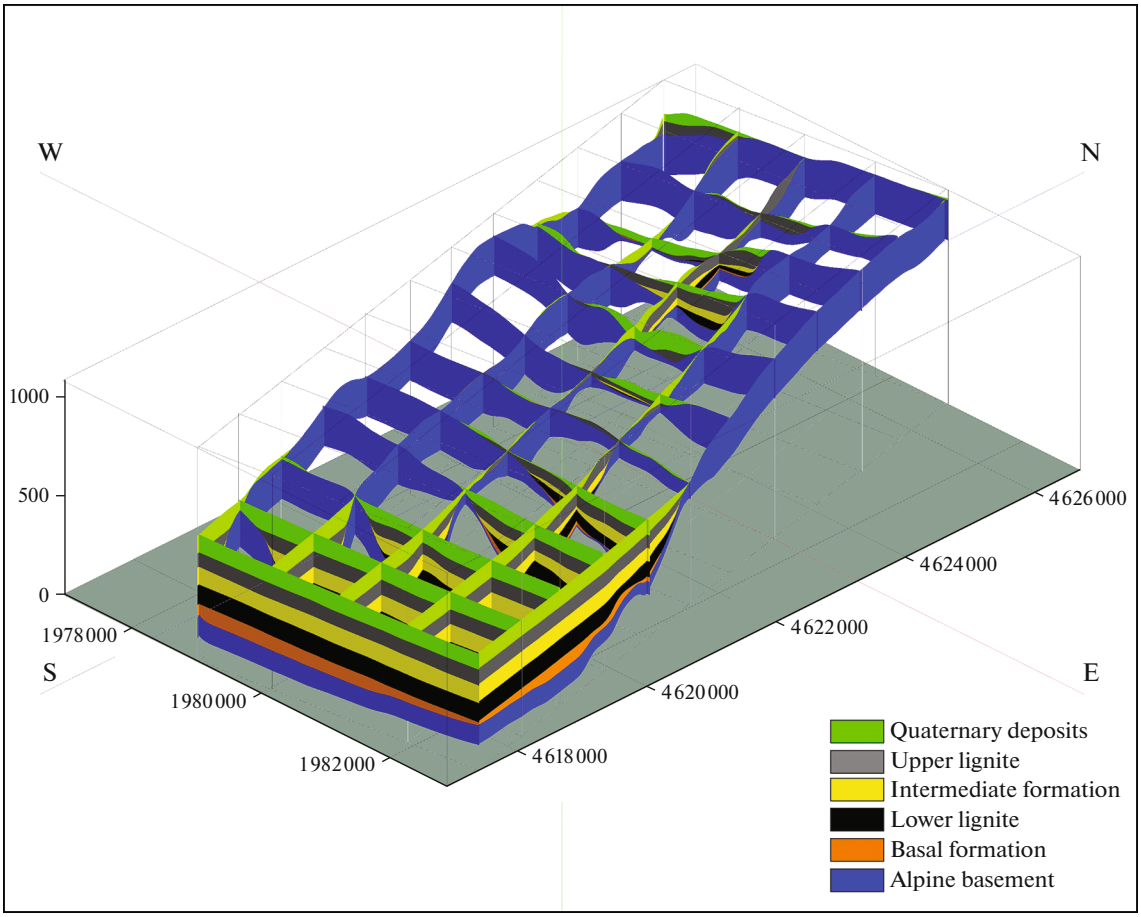

Fig. 4. 3D image of the Kleidi basin in the form of fence-diagram, derived from the inverse-distance (*ID*) interpolation (after [36]).

southern graben being larger and lying lower than the northern one. The geometry of the basal contact, as well as the contact layer surfaces, seem rather undulating. The lower and upper lignite marker horizons are shown in dark grey and light grey, respectively (Figs. 3 and 5). Figure 6 illustrates the interpolated thicknesses per cored formation. The basal formation (which overlies the basement) starts as a thin veneer in the northern basin but thickens southwards. In contrast, the overlying deposits (lower lignite, intermediate formation, upper lignite) exhibit notable thicknesses both in the northern and southern grabens but in different proportions. The upper lignite exhibits greater thickness than the lower lignite in the northern graben but their thicknesses are similar in the southern graben. Numerical differential geometry methods have been applied to digital terrain models (DTM) to identify tectonic phenomena [9]. Here, the thickness fluctuations were further examined by derivation in two dimensions of the calculated thickness rasters (Fig. 7, slope of the thickness).

The slope zones out parts of each formation with drastically reduced (or increased) thickness compared to their surroundings (Fig. 7). Furthermore, the second derivative (curvature) of the thickness raster delineates breaks in the slope, which represent either local thickening (negative curvature) or local thinning (positive curvature) of the interpolated layers (Fig. 8).

RESULTS AND DISCUSSION

The thickness of the interpolated strata shown in the geological cross-sections is not uniform across the entire basin (north and south grabens), and deviations from uniformity should be attributed to structural perturbations of the basin (Figs. 4, 5). The derivation products not only zone out regions of change but also delineate the breaks in the thickness (Figs. 7, 8). Marked breaks in the stratigraphic thickness obviously trace the faults responsible for the change (Fig. 8). Faults may either favor apparent thickness accumulation or apparent thinning of the strata (via shearing), depending on whether a synrift or a postrift sequence is intersected [34, 35]. Based on that, it turns out that the Kleidi basin underwent non-uniform rifting over the Neogene and the certain faults were growing while others were not.

In the southern graben the inferred faults generally trend in a WNW–ENE and NE–SW direction. Here, the Neogene deposits demonstrate their greatest

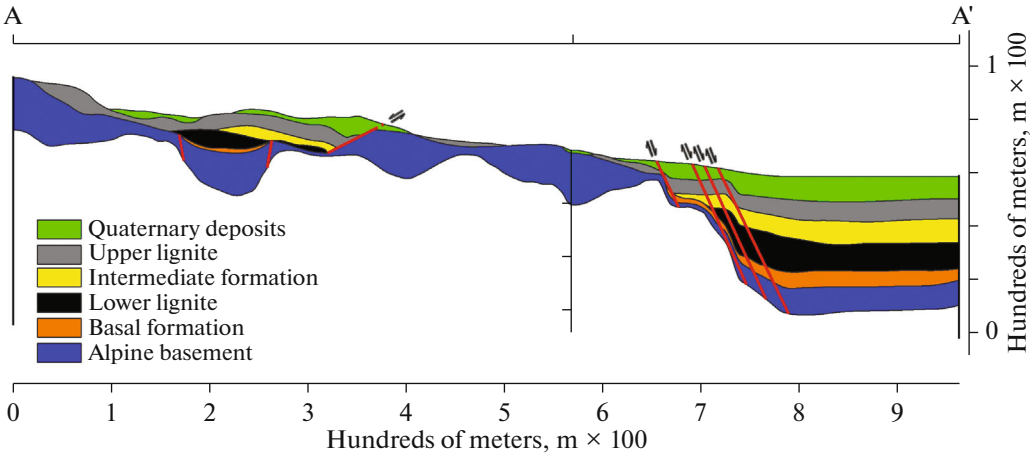

Fig. 5. North-south geological section (A–A') of the Kleidi basin, generated through interpolation of the stratigraphic horizons recorded in the boreholes. Units on the horizontal and vertical axes are hundreds of meters (m).

thickness (Fig. 8). They appear undeformed for the most part of the southern graben but exhibit substantial deformation in the northern shoulder of the graben, where the basal formation and the lower lignite are being flexed towards parallelism with the graben wall. The curvature of these strata is consistent with a synrift sequence and fault propagation folding functioning at the shoulder of the graben. The apparent fault throw progressively decreases upsection, from ~400 m for the basement/basal formation boundary (and even greater if the drag is added to the discrete fault displacement) to <50 m on the Upper lignite/Quaternary boundary. Therefore, progressive accumulation of throw downsection reveals the synrift character of the sequence and uninterrupted neotectonic activity and continuous subsidence in the southern graben until at least the beginning of the Quaternary. Fault activity, and the resulting subsidence rate, was probably intensified in the Upper Miocene, as shown from the increased true thickness of the lower lignite in the hanging wall. The stratigraphy is sequentially smearing-out towards the south over a distance of ~50–100 m, implying that the layers are being caught between a series of overlapping deformation bands of extensional mode (Fig. 5). Although coal generally behaves brittlely, the high clay content renders the layers weak enough to become smeared-out. Next, the deposits continue almost undisturbed, presenting uninterrupted the entire Upper Miocene–Quaternary sequence while preserving the thicknesses. Synrift offsets should also be occurring in this part of the graben, but they are not discernible at the resolution of the cross-section.

Tectonostratigraphy in the northern graben follows a different pattern. The Neogene stratigraphy appears intermittent. The Upper Miocene–Lower Pliocene deposits (basal formation, lower lignite, intermediate formation) are limited to the center of the graben but with markedly lower thicknesses than their counterparts in the southern basin (Figs. 5, 6). However, the Plio-Quaternary fill (upper lignite and Quaternary deposits) exhibits greater lateral expanse, onlaping the underlying Mio-Pliocene deposits and the graben shoulders from end to end, and share similar thicknesses with their southern equivalents. This observation suggests that the northern graben was rather narrow during the Upper Miocene, but rifting accelerated during Pliocene–Lower Quaternary, substantially widening the graben to its present dimensions (Fig. 6, expanse of the basal formation and lower lignite). Pairs of parallel NE–SW and NW–SE trending faults encircle (almost like ring faults) the graben (Fig. 8). Moreover, the strata in the northern graben appear slightly tilted southwards, whereas the Mio-Pliocene deposits shear out towards the southern wall of the northern graben. These observations imply that a listric fault might have been functioning in the southern wall of the northern graben, rotating and thinning the strata southwards through vertical simple shear in a rollover anticline.

Nevertheless, the intensified tectonic deepening observed in the southern graben during the Miocene (reflected on the stratigraphic thickening of the lower lignite in the hanging wall) has no equivalent in the northern graben. There, substantial structural remodeling occurs later, on the Pliocene/Quaternary boundary where graben-widening dominated over graben-deepening. In essence, the kinematics of the individual grabens of the Kleidi basin seems to have been independent one from the other during the Neogene. The chronostratigraphy relates much of the structural configuration of the southern graben with the Late Miocene extensional event [25], which formed much of the broader Ptolemais basin.

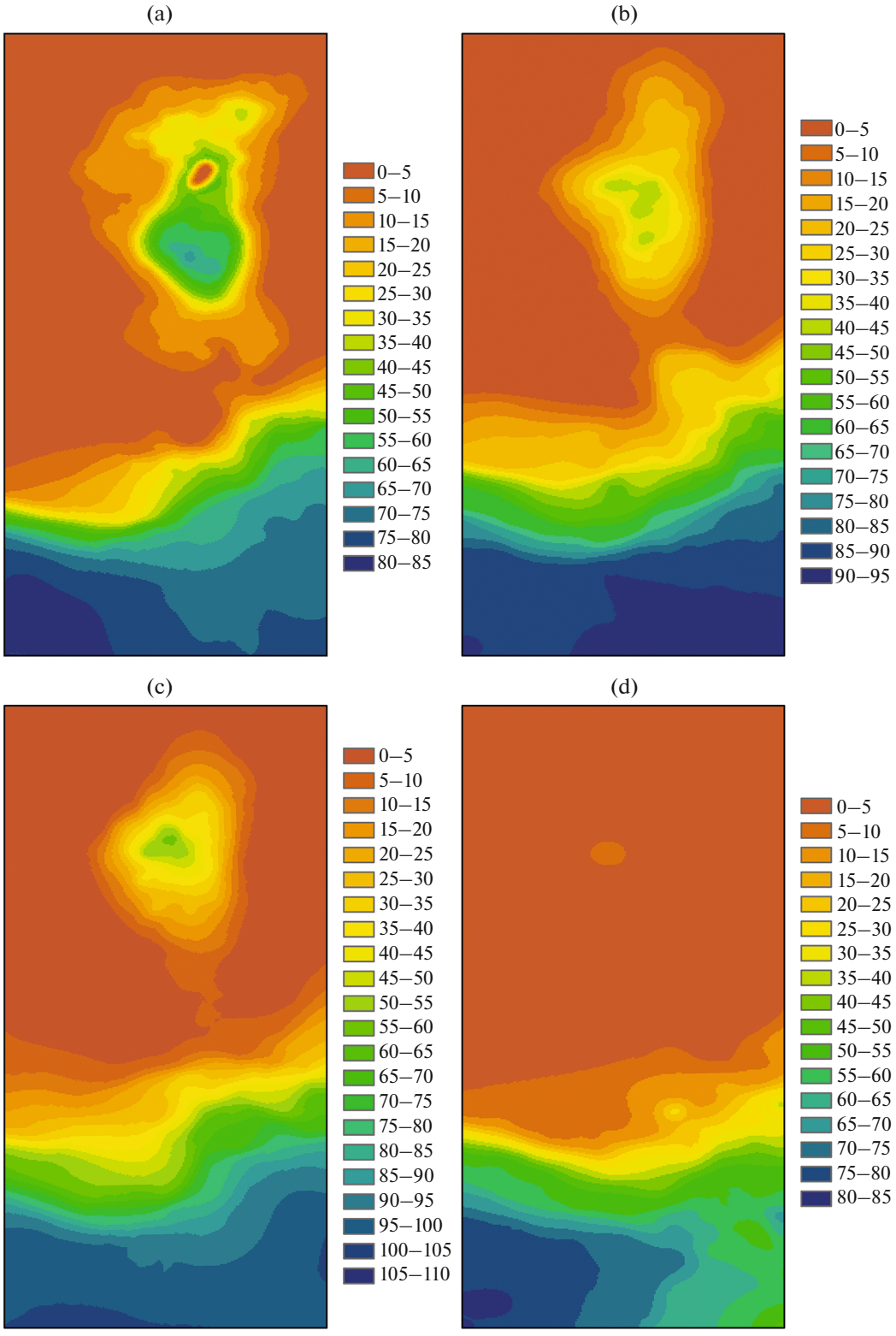

Fig. 6. Interpolated thicknesses for the lithologies. (a) Upper lignite; (b) Intermediate formation; (c) Lower lignite; (d) Base formation. Unit on the vertical axis is meters (m).

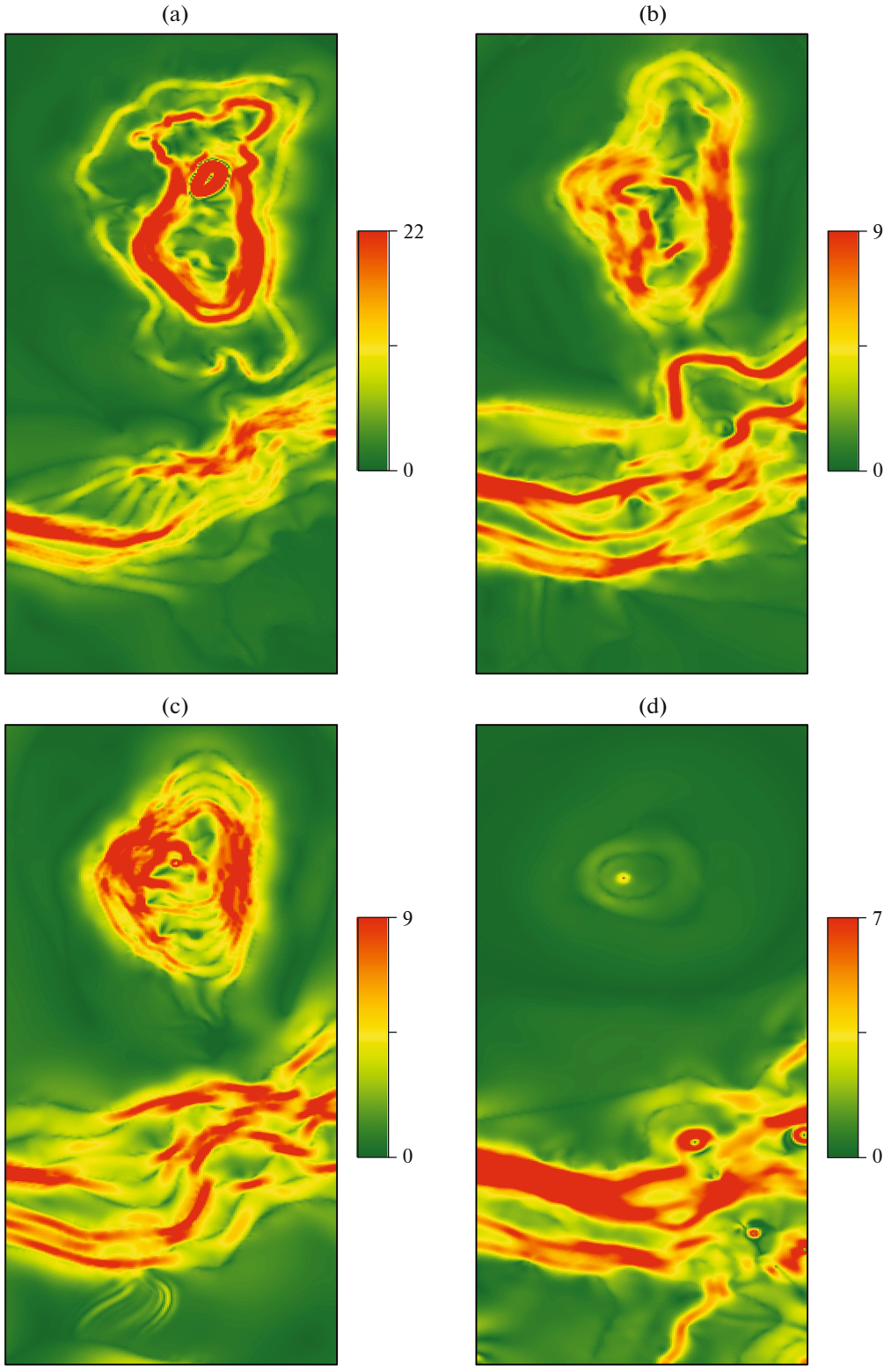

Fig. 7. The first derivative (slope) of (a) Upper lignite, (b) Intermediate formation, (c) Lower lignite, (d) Base formation. The unit of the color-graded scale is degrees. For the thickness of each formation see Fig. 6.

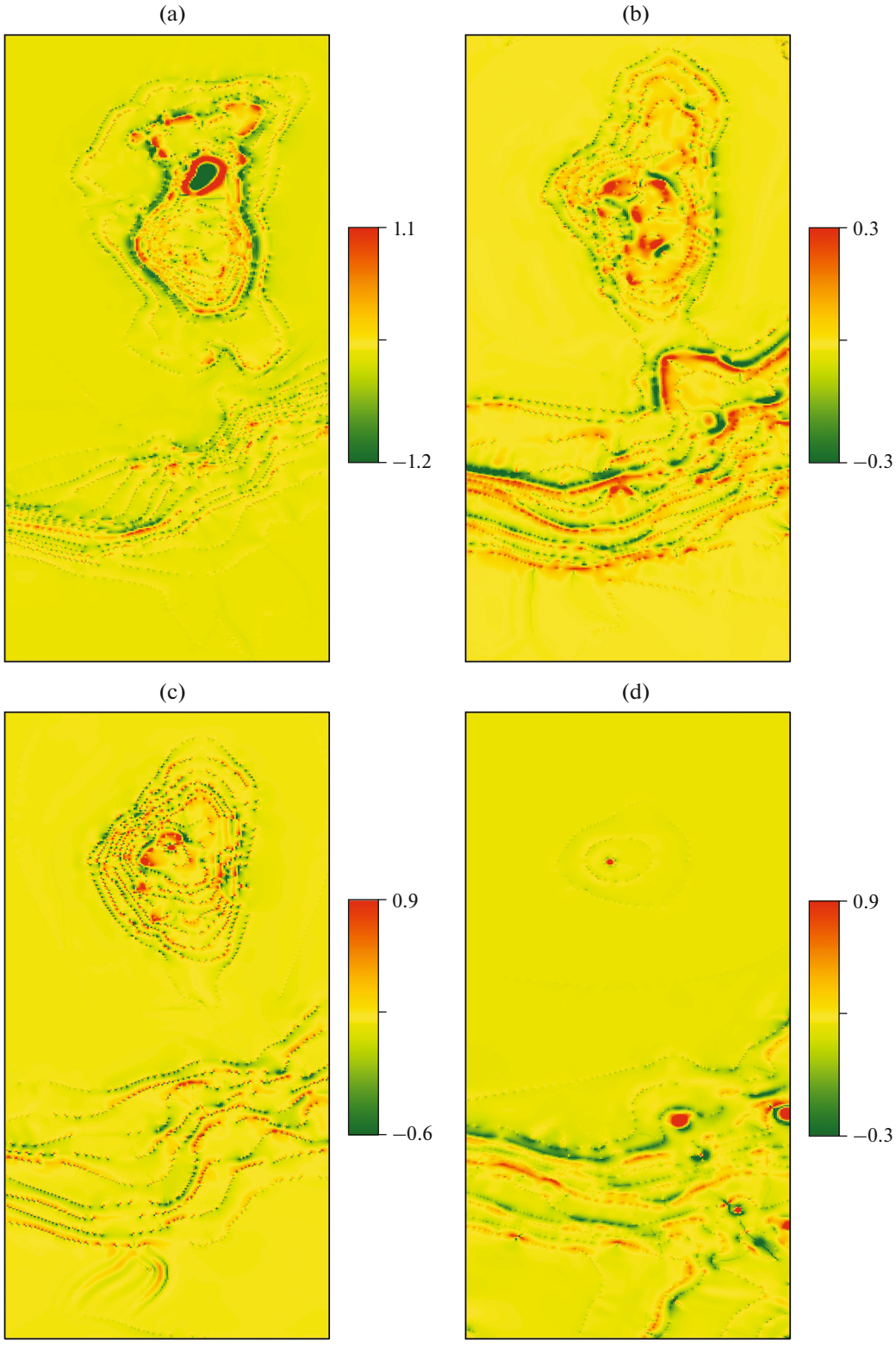

Fig. 8. The second derivative (curvature) given in percentage of (a) Upper lignite, (b) Intermediate formation, (c) Lower lignite, (d) Base formation. Breaks in curvature delineate probable faults. For the thickness of each formation see Fig. 6.

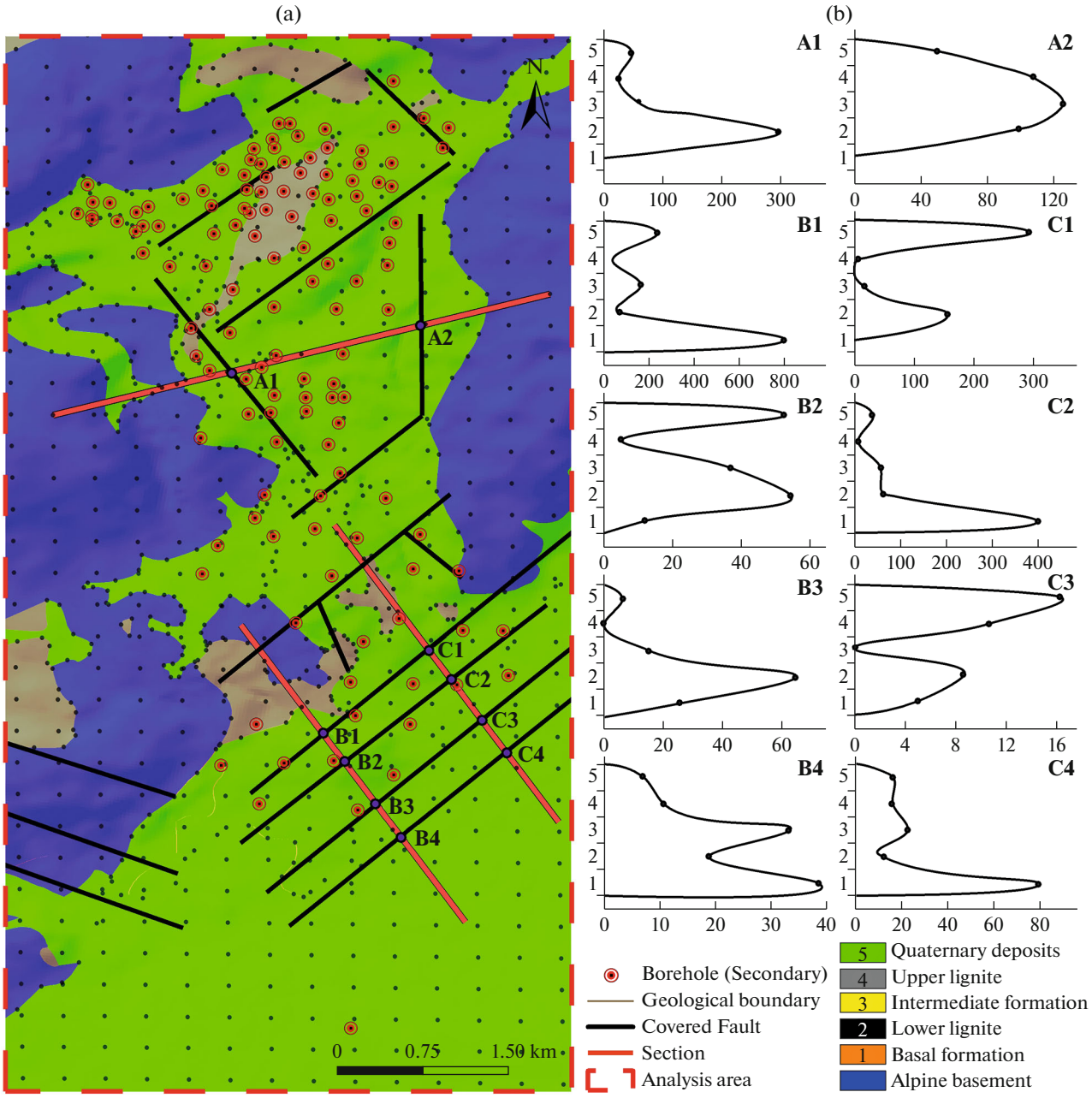

Fig. 9. Prominent faults of northern and southern grabens of the Kleidi sedimentary basin (a); percentage of stratigraphic interval change versus chronostratigraphy (b). The horizontal axis provides the percentage of stratigraphic interval change (net values) and the vertical axis the chronostratigraphy.

Similar associations in the northern basin relate most of its widening with the Late Pliocene–Quaternary extensional phase [25].

Figure 9 illustrates prominent faults of the northern and the southern grabens, selected from those resulting from the previous process, that were used to calculate the percentage of stratigraphic interval change (I) by measuring the thickness of each bed perpendicular to the fault following the Inverse-Distance (ID) method [36]. The two major phases of fault growth documented in the broader area can be recognized in almost all cases [17, 25] (Fig. 9). The parameter I reaches its highest value in the basal formation and the lower lignite (Fig. 9b, lower peaks), suggesting that the basin underwent considerable rifting during the Upper Miocene. The subsequent phase of rifting during the Plio-Quaternary is reflected on all measured spots, but its intensity is somewhat uneven across the basin with some faults having produced greater throw (i.e. large values of percentage of stratigraphic interval change)

while some others were only slightly offset. Another subtle peak occasionally crops up between the previously recognized pronounced peaks in plots referring to the southern graben (B1, C2, B4, C4), but it is absent from similar plots for the northern graben. This Pliocene event (Intermediate formation) may echo a smaller, but so far unknown from the regional record, phase of tectonic recrudescence that mainly affected the southern graben and points to the conclusion of the first (Miocene) deformation phase.

CONCLUSIONS

(1) Our study introduces a new perspective to the neotectonic framework of the broader Ptolemais basin, replacing the shortage of direct morphotectonic field evidence with structural analysis of a rift basin. Particularly, the Kleidi basin is part of the broader Ptolemais Basin in Western Macedonia (Greece). Boreholes retrieved by the Geological and Mineral Exploration ((IGME), Athens, Greece) and Public Power Corporation of Greece ((PPC), Athens, Greece) demonstrate continuous sedimentation from the Upper Miocene to the Middle Quaternary. The intra-basin Neogene deposits tend to thicken towards the SE. Coring also revealed a subsurface ridge of the basement, which divides the basin into the northern and the southern grabens. The southern graben being larger and lying lower than the northern graben.

(2) Lithostratigraphic data were interpolated using the inverse distance algorithm (ID method). The resulting thickness rasters were submitted to successive derivations (slope and curvature), allowing the discovery of a number of faults. The stratigraphic architecture, as well as the deformation pattern, seems to be different between the two grabens. In the southern graben, the Neogene deposits demonstrate greater thickness and continuous tectonic subsidence, heightened on the Miocene–Pliocene boundary and resulting in an accumulated throw of at least 400 m. In the northern graben the equivalent deposits appear underdeveloped, while rifting seems to have favored the widening of the northern graben (in contrast to the deepening of the southern graben), which was intensified during Pliocene–Lower Quaternary.

(3) The intensified deformation episodes recorded in the southern and northern grabens, dated to Upper Miocene–Pliocene and Pliocene–Middle Quaternary respectively, echo the two principal extension phases that have been recognized in the Ptolemais basin and the broader area. Besides, careful analysis of the coring data may tentatively point to a third, and so far undocumented, phase of subtle tectonic recrudescence in the NE Ptolemains sedimentary basin during the Pliocene.

AKNOWLEDGMENTS

Authors are grateful to anonymous reviewers for their helpful comments.

Authors thank the Public Power Corporation S.A., Mining Engineering Department (PPC, Athens, Greece), for making available reports and coring data for analysis.

CONFLICT OF INTEREST

The authors declare that they have no conflicts of interest.

REFERENCES

1. J. Anastopoulos and N. Koukouzas, "Economic geology of the southern part of Ptolemais lignite basin (Macedonia–Greece)," Geol. Geophys. Res. (IGME, Athens) **XVI** (1), (1972) [in Greek].
2. A. Beach, "Structural evolution of the Witch Ground Graben," J. Geol. Soc. London **141**, 621–628 (1984).
3. E. Delogkos, C. Childs, T. Manzocchi, and J. J. Walsh, "The nature and origin of bed-parallel slip in Kardia Mine, Ptolemais Basin, Greece," J. Struct. Geol. **113**, 115–133 (2018).
4. M. Goldsworthy, J. Jackson, and J. Haines, "The continuity of active fault systems in Greece," Geophys. J. Int. **148**, 596–618 (2002).
5. A. Gibbs, "Structural evolution of extensional basin margins," J. Geol. Soc. London **141**, 609–620 (1984). https://doi.org/10.1144/gsjgs.141.4.0609
6. K. Hatzisavvas, *Geological–Geotechnical Study of Kleidi Mine* (Public Power Corp. Greece, Mining Eng. Depart., Sect. Hydrogeol., Greece, 2012).
7. K. Hatzisavvas and P. Skilitzis, *Geological–Soil Technical Illustration of Kleidi Mine* (Public Power Corp. Greece, Mining Eng. Depart., Sect. Hydrogeol., Greece, 2004).
8. W.S. Hou, L. Yang, D. C. Deng, J. Ye, K. Clarke, Z. J. Yang, W. M. Zhuang, J. X. Liu, and J. C. Huang, "Assessing quality of urban underground spaces by coupling 3D geological models: The case study of Foshan City, South China," Comp. Geosci. **89**, 1–11 (2016).
9. G. Jordan, B. M. L. Meijninger, D. J. J. van Hinsbergen, J. E. Meulenkamp, and P. M. van Dijk, "Extraction of morphotectonic features from DEMs: Development and applications for study areas in Hungary and NW Greece," Int. J. Appl. Earth Observ. Geoinformat., No. 7, 163–182 (2005).
10. K. N. Koukouzas, *The 1 : 50000 Geological Map of Greece, Ptolemais Sheet* (Inst. Geol. Miner. Explor. (IGME), Athens, 1995).
11. K. Koukouzas, Th. Kotis, M. Ploumidis, A. Metaxas, and D. Dimitriou, "Lignite deposits of Ptolemaida trench," in *Proceedings of International Meeting "Exploitation of Low Energy Solid Fuel"* (DEH, Ptolemaida, Greece, 1985), pp. 1–10 [in Greek].
12. C. Koukouzas and N. Koukouzas, "Coals from Greece: Distribution, quality and reserves," in *European Coal Geology,* Ed. by M. K. G. Whateley and D. A. Spears (Spec. Publ.—Geol. Soc. London, 1995. Vol. 82), pp. 171–180.

13. Th. Kotis, M. Ploumidis, A. Metaxas, and G. Varvarousi, *Sedimentological Study of Lignite Deposit in Kleidi Area of Florina* (Inst. Geol. Miner. Explor. (IGME), Athens, 1997) [in Greek].
14. S. E. Laubach, J. Lamarche, B. D. M. Gauthier, W. M. Dunne, and D. J. Sanderson, "Spatial arrangement of faults and opening-mode fractures," J. Struct. Geol. **108**, 2–15 (2018).
15. H. Liu, S. Chen, M. Hou, and L. He, "Improved inverse distance weighting method application considering spatial autocorrelation in 3D geological modeling," Earth Sci. Inform. **13**, 619–632 (2020).
16. G. Louloudis, C. Roumpos, K. Theofilogiannakos, and N. Stathopoulos, "Multi-seam coal deposit modeling via principle component analysis and GIS," Minerals **9** (532), 1–23 (2019). https://doi.org/10.3390/min9090532
17. J. L. Mercier, D. Sorel, P. Vergely, and K. Simeakis, "Extensional tectonic regimes in the Aegean basins during the Cenozoic," Basin Res. **2**, 49–71 (1989). https://doi.org/10.1111/J.1365-2117.1989.TB00026.X
18. D. Mountrakis, S. Pavlides, N. Zouros, T. Astaras, and A. Chatzipetros, "Seismic fault geometry and kinematics of the 13 May 1995 western Macedonia (Greece) earthquake," J. Geodynam. **26**, 175–196 (1998). https://doi.org/10.1016/S0264-3707(97)00082-3
19. J. Muzik, T. Vondráčkvá, D. Sitányiová, J. Plachý, and V. Nývlt, "Creation of 3D geological models using interpolation methods for numerical modeling," Proc. Earth Planet. Sci. **15**, 25–30 (2015). https://doi.org/10.1016/J.PROEPS.2015.08.007
20. D. Ntokos, "Neotectonic study of Northwestern Greece," J. Maps **14**, 178–188 (2018). https://doi.org/10.1080/17445647.2018.1445562
21. D. Ntokos, "Age estimation of tectonically exposed surfaces using cation-ratio dating of rock varnish," CATENA **200** (105167), 1–10 (2021). https://doi.org/10.1016/j.catena.2021.105167
22. I. Oikonomopoulos, G. Kaouras, P. Antoniadis, T. Perraki, and H. J. Gregor, "Neogene Achlada lignite deposits in NW Greece," Bull. Geosci. **83**, 335–338 (2008).
23. C. Orfanos, K. Leontarakis, G. Apostolopoulos, C. Athanassas, and P. Kofakis, "Preparation study based on borehole data for Delphi–Distomon mining area to better design geophysical works," in *Proceedings of the 2nd Conference on Geophysics for Mineral Exploration and Mining, Sept. 2018,* Vol. 2018, pp. 1–5. https://doi.org/10.3997/2214-4609.201802710
24. S. B. Pavlides, *Neotectonic Evolution of the Florina-Vegoritis-Ptolemais basins. PhD Thesis* (Univ. Thessaloniki, Thessaloniki, Greece. 1985) [in Greek].
25. S. B. Pavlides and D. M. Mountrakis, "Extensional tectonics of northwestern Macedonia, Greece, since the late Miocene," J. Struct. Geol. **9**, 385–392 (1987). https://doi.org/10.1016/0191-8141%2887%2990115-5
26. S. B. Pavlides, N. C. Zouros, A. A. Chatzipetros, D. S. Kostopoulos, and D. M. Mountrakis, "The 13 May 1995 western Macedonia, Greece (Kozani Grevena) earthquake; preliminary results", Terra Nova, No. 7, 544–549 (1995). https://doi.org/10.1111/J.1365-3121.1995.TB00556.X
27. J. H. Rippon, "Contoured patterns of the throw and hade of normal faults in the Coal Measures (Westphalian) of north-east Derbyshire," Proc. Yorkshire Geol. Soc. **45**, 147–161 (1985).
28. J. Steenbrink, N. Van Vugt, F. J. Hilgen, J. R. Wijbrans, and J. E. Meulenkamp, "Sedimentary cycles and volcanic ash beds in the Lower Pliocene lacustrine succession of Ptolemais (NW Greece): Discrepancy between $^{40}Ar/^{39}Ar$ and astronomical ages," Palaeogeogr., Palaeoclimatol., Palaeoecol. **152**, 283–303 (1999). https://doi.org/10.1016/S0031-0182%2899%2900044-9
29. N. Van Vugt, J. Steenbrink, C. G. Langereis, F. J. Hilgen, and J. E. Meulenkamp, "Magnetostratigraphy-based astronomical tuning of the early Pliocene lacustrine sediments of Ptolemais (NW Greece) and bed-to-bed correlation with the marine record," Earth Planet Sci. Lett. **164**, 535–551 (1998). https://doi.org/10.1016/S0012-821X%2898%2900236-2
30. E. Velitzeos and I. Petrescu, "Rare plant fossils from the Neogene ligniferous basin of Vegora," Ann. Géol. Pays. Hellen. **30**, 767–777 (1981).
31. J. J. Walsh and J. Watterson, "Distributions of cumulative displacement and seismic slip on a single normal fault surface," J. Struct. Geol. **9**, 1039–1046 (1987).
32. J. J. Walsh and J. Watterson, "Analysis of the relationship between displacements and dimensions of faults," J. Struct. Geol. **3**, 239–247 (1988).
33. C. Wang, G. W. Wang, J. S. Liou, and D. H. Zhang, "3D geochemical modeling for subsurface targets of Dashui au deposit in Western Qinling (China)," J. Geochem. Explor. **203**, 59–77 (2019).
34. X. Wang, "Uncertainty quantification and reduction in the characterization of subsurface stratigraphy using limited geotechnical investigation data," Underground Space **5**, 124–143 (2020).
35. C. D. Williams, C. M. Powell, and M. A. Cooper, "Geometry and kinematics of inversion tectonics," Spec. Publ.—Geol. Soc. London **44**, 3–15 (1989).
36. RockWare: Earth Science Software, Consulting, and Traiuning. https://www.rockware.com. Accessed May 21, 2021.